Impurity effects on electrical conductivity of doped bilayer graphene in the presence of a bias voltage

E Lotfi[1,†], H Rezania[2], B Arghavaninia[3], and M Yarmohammadi[4]

[1] Department of Physics, Sanandaj Branch, Islamic Azad University, Sanandaj, Iran
[2] Department of Physics, Razi University, Kermanshah, Iran
[3] Department of Physics, Kermanshah Branch, Islamic Azad University, Kermanshah, Iran
[4] Young researchers and Elite Club, Kermanshah Branch, Islamic Azad University, Kermanshah, Iran

(Received 25 January 2016; revised manuscript received 15 March 2016; published online 27 May 2016)

We address the electrical conductivity of bilayer graphene as a function of temperature, impurity concentration, and scattering strength in the presence of a finite bias voltage at finite doping, beginning with a description of the tight-binding model using the linear response theory and Green's function approach. Our results show a linear behavior at high doping for the case of high bias voltage. The effects of electron doping on the electrical conductivity have been studied via changing the electronic chemical potential. We also discuss and analyze how the bias voltage affects the temperature behavior of the electrical conductivity. Finally, we study the behavior of the electrical conductivity as a function of the impurity concentration and scattering strength for different bias voltages and chemical potentials respectively. The electrical conductivity is found to be monotonically decreasing with impurity scattering strength due to the increased scattering among electrons at higher impurity scattering strength.

Keywords: bilayer graphene, Green's function, electrical conductivity

PACS: 61.46.–w, 62.25.–g, 61.46.Hk, 71.10.–w **DOI:** 10.1088/1674-1056/25/7/076102

1. Introduction

Electrons in bilayer graphene exhibit quite unusual properties: they can be viewed as massive chiral fermions with a parabolic dispersion at intermediate energies and have Berry phase 2π;[1,2] in contrast, the charge carriers in monolayer graphene are Berry-phase-π quasiparticles with a linear dispersion.[3,4] In bilayer graphene (BLG), two coupled hexagonal lattices of carbon atoms are arranged according to simple and Bernal stacking.[1,5–9] Because BLG has a large degeneracy at the charge neutral point,[1,5–9] there have been intense discussions on the possible many-body effects in the system.[10–15] Moreover, since electrons in single layer graphene (SLG) behave as relativistic massless fermions,[9] BLG provides a unique play ground to control the interactions between relativistic particles and relative mechanical motions of two layers. The electronic structure of bilayer graphene was studied theoretically and the spectrum was found to be essentially different from that of monolayer graphene.[1] In addition to interesting underlying physics, bilayer graphene holds potential for electronic applications, not only because of the possibility to control both carrier density and energy band gap through doping or gating.[1,8,16–20] Not surprisingly, many of the properties of bilayer graphene are similar to those of monolayer graphene.[9,21] These include an excellent electrical conductivity with room temperature mobility up to 40000 $\mathrm{cm}^2 \cdot \mathrm{V}^{-1} \cdot \mathrm{s}^{-1}$ in air,[22] the possibility to tune the electrical properties by changing the carrier density through gating or doping,[17,23,24] a high thermal conductivity with room temperature thermal conductivity about 2800 $\mathrm{W} \cdot \mathrm{m}^{-1} \cdot \mathrm{K}^{-1}$,[25,26] mechanical stiffness, strength, flexibility (Young's modulus is estimated to be about 0.8 TPa[27,28]), transparency with transmittance of white light of about 95%,[29] impermeability to gases,[30] and the ability to be chemically functionalised.[31] Thus, as monolayer graphene, bilayer graphene has potentials for future applications in many areas,[21] including transparent, flexible electrodes for touch screen displays,[32] high-frequency transistors,[33] thermoelectric devices,[34] plasmonic devices,[35] photodetectors,[36] batteries,[37,38] and composite materials.[39,40] It should be stressed, however, that bilayer graphene has features that make it distinct from monolayer graphene. Like monolayer graphene, intrinsic bilayer graphene has no band gap between its conduction and valence bands, but the low-energy dispersion is quadratic (rather than linear in monolayer graphene) with massive chiral quasiparticles[1,2] rather than massless ones. As there are only two layers, bilayer graphene represents the thinnest limit of an intercalated material.[37,38] It is possible to address each layer separately leading to entirely new functionalities in bilayer graphene, including the possibility to control an energy band gap of up to about 300 meV through doping or gating.[1,8,16–20]

In contrast to the case of SLG, low energy excitations of the bilayer graphene have a parabolic spectrum, although the chiral form of the effective two-band Hamiltonian persists

†Corresponding author. E-mail: lotfi.erf@gmail.com

© 2016 Chinese Physical Society and IOP Publishing Ltd

because the sublattice pseudospin is still a relevant degree of freedom. The low energy approximation in bilayer graphene is valid only for small doping $n < 10^{12}$ cm^{-2}, while experimentally doping can obtain 10 times larger densities. For such a large doping, the 4-band model[1] should be used instead of the low energy effective two-band model. Bilayer graphene is of intense interest as it too shows an unusual quantum Hall effect[1,41] and indeed its low energy tight-binding Hamiltonian maps to an equation for chiral fermions with an effective mass based on an interlayer hopping parameter γ. Graphene is an extremely flexible material from the electronic point of view and the electronic gap can be controlled. This can be accomplished in a graphene bilayer with an electric field applied perpendicular to the plane. It was shown theoretically[1,18] and demonstrated experimentally[20,42] that the graphene bilayer is the only material with semiconducting properties that can be controlled by the electric field effect.[8] The gap between the conduction and valence bands is proportional to the voltage drop between the two graphene planes and can be as large as 0.1–0.3 eV, allowing for novel THz devices[20] and carbon based quantum dots[43] and transistors.[44] Bilayer graphene is sensitive to the unavoidable disorder generated by the environment of the SiO_2 substrate: adatoms, ionized impurities, etc. In this context, it is worth mentioning the transport theories based on the Boltzman equation,[45] a study of weak localization in bilayer graphene,[46] and also the corresponding further experimental characterization.[47] The static transport in few-layer graphene has been studied for both without and in the presence of a magnetic field. Thermopower of clean and impure biased bilayer graphene has been calculated for Bernal AB-stacking within the Born approximation.[48]

In our previous work, we studied the transport properties of clean bilayer graphene in the presence of a biased voltage.[49,50] In this paper, we study the effects of site dilution or unitary scattering and bias voltage on the electrical conductivity of both AA and AB stacked graphene bilayers within the well-known self-consistent Born approximation (SCBA).[48] This approximation allows for analytical results of electronic self-energies, allowing us to compute physical quantities such as spectral functions measured by angle resolved photoemission[51,52] and density of states measured by scanning tunneling microscopy,[53,54] besides the standard transport properties such as the direct-current (DC) and alternating-current (AC) conductivities. To ensure the applicability of SCBA, we restrict our calculations to relatively clean systems with low impurity concentrations. The electrical conductivity of two different stacked bilayer graphene as a function of the impurity concentration is calculated for different bias voltages and scattering potential strengths. We also study the effects of the impurity concentration and scattering potential strength on the temperature dependence of the electrical conductivity in bilayer grapehene.

2. Theoretical method and formalism

We start from a tight-binding model incorporating the nearest neighboring intralayer and interlayer hopping terms. An on-site potential energy difference between the two layers is included to model the effect of an external voltage. For the case of AA-stacking,[44] an A (B) atom in the upper layer is stacked directly above the A (B) atom in the lower layer. The nearest neighbor tight-binding model Hamiltonians for AA-stacked bilayer grapehene ($H_{\rm AA}^{\rm T.B}$) and AB one ($H_{\rm AB}^{\rm T.B}$) are given as

$$\begin{aligned} H_{\rm AA}^{\rm T.B} &= -t_{\|}\sum_{i,l,\delta}(b_{l,i+\delta}^{\dagger}a_{l,i}+{\rm h.c.})+\gamma\sum_{i}(a_{1,i}^{\dagger}a_{2,i}+{\rm h.c.}) \\ &\quad +\gamma\sum_{i}(b_{1,i}^{\dagger}b_{2,i}+{\rm h.c.}) \\ &\quad +\frac{V}{2}\sum_{i}(a_{1,i}^{\dagger}a_{1,i}+b_{1,i}^{\dagger}b_{1,i}-a_{2,i}^{\dagger}a_{2,i}-b_{2,i}^{\dagger}b_{2,i}), \\ H_{\rm AB}^{\rm T.B} &= -t_{\|}\sum_{i,l,\delta}(b_{l,i+\delta}^{\dagger}a_{l,i}+{\rm h.c.})+\gamma\sum_{i}(b_{1,i}^{\dagger}a_{2,i}+{\rm h.c.}) \\ &\quad +\frac{V}{2}\sum_{i}(a_{1,i}^{\dagger}a_{1,i}+b_{1,i}^{\dagger}b_{1,i}-a_{2,i}^{\dagger}a_{2,i}-b_{2,i}^{\dagger}b_{2,i}). \end{aligned} \quad (1)$$

The first two terms are the nearest neighbor intralayer hopping terms for electrons to move within a given plane with hopping energy $t_{\|}\approx 3$ eV. The two planes are indexed by 1 and 2. According to the crystal structure of the honeycomb lattice, each layer has two inequivalent atoms labeled as A and B. The lattice structures of bilayer grapehene and single-layer grapehene are shown in Figs. 1 and 2, respectively. The unit cell vectors of bilayer graphene which are similar to those of single-layer grapehene are given by

$$\boldsymbol{a}_1=-a\hat{\boldsymbol{j}}, \qquad \boldsymbol{a}_2=\frac{a}{2}(\hat{\boldsymbol{j}}+\sqrt{3}\hat{\boldsymbol{i}}), \quad (2)$$

where $\hat{\boldsymbol{i}}$ and $\hat{\boldsymbol{j}}$ are the unit vectors along x and y directions, respectively. In Eq. (1), $a_{l,i}$ denotes the annihilation operator for an electron on an A site with site label i in graphene layer l, $b_{l,i+\delta}^{\dagger}$ creates an electron in layer l on the neighboring site at position $i+\delta$, where δ is one of the three possible nearest-neighbor vectors $\boldsymbol{a}_{01}$, $\boldsymbol{a}_{02}$, and $\boldsymbol{a}_{03}$ which are shown in Fig. 1. Furthermore, the primitive vectors of the triangular sublattice have property $|\boldsymbol{a}_1|=|\boldsymbol{a}_2|=\sqrt{3}a_{\rm cc}$ with $a_{\rm cc}$ the nearest carbon–carbon distance. The third term in Eq. (1) corresponds to the interlayer hopping between the graphene layers. The hopping parameter between an A or B atom site in one layer and the nearest A or B atom site in the other layer is given by γ and is reported to be about 0.2 eV.[31,32] The V is the potential energy difference between the first and the second layers induced by a bias voltage. In terms of Fourier transformation of operators, one can rewrite the clean tight binding

part of the Hamiltonian in Eq. (1) as

$$H_{\mathrm{AA(AB)}} = \sum_{\boldsymbol{k}} \phi^{\dagger}_{\boldsymbol{k}} H^{\mathrm{T.B}}_{\mathrm{AA(AB)}}(\boldsymbol{k}) \phi_{\boldsymbol{k}}, \tag{3}$$

in which the vector of fermion creation operators is defined as $\phi^{\dagger}_{\boldsymbol{k}} = (a^{\dagger}_{1,\boldsymbol{k}}, b^{\dagger}_{2,\boldsymbol{k}}, a^{\dagger}_{2,\boldsymbol{k}}, b^{\dagger}_{1,\boldsymbol{k}})$, where $a^{\dagger}_{l,\boldsymbol{k}}$ and $b^{\dagger}_{l,\boldsymbol{k}}$ are the Fourier transformations of $a^{\dagger}_{l,i}$ and $b^{\dagger}_{l,i}$, respectively. The Fourier transformations are expressed as

$$\begin{aligned} a^{\dagger}_{l,\boldsymbol{k}} &= \frac{1}{\sqrt{N}} \sum_{i} \mathrm{e}^{-\mathrm{i}\boldsymbol{k}\cdot\boldsymbol{R}_i} a^{\dagger}_{l,i}, \\ b^{\dagger}_{l,\boldsymbol{k}} &= \frac{1}{\sqrt{N}} \sum_{i} \mathrm{e}^{-\mathrm{i}\boldsymbol{k}\cdot\boldsymbol{R}_i} b^{\dagger}_{l,i}, \end{aligned}$$

where N is the number of unit cells and $\boldsymbol{k}$ is the wave vector belonging to the first Brillouin zone of the honeycomb structure. The nearest neighbor approximation gives us the following matrix forms for $H^{\mathrm{T.B}}_{\mathrm{AA}}(\boldsymbol{k})$ and $H^{\mathrm{T.B}}_{\mathrm{AB}}(\boldsymbol{k})$:

$$\begin{aligned} H^{\mathrm{T.B}}_{\mathrm{AA}}(\boldsymbol{k}) &= \begin{pmatrix} V/2 & 0 & \gamma & f(\boldsymbol{k}) \\ 0 & V/2 & f^{*}(\boldsymbol{k}) & \gamma \\ \gamma & f(\boldsymbol{k}) & -V/2 & 0 \\ f^{*}(\boldsymbol{k}) & \gamma & 0 & -V/2 \end{pmatrix}, \\ H^{\mathrm{T.B}}_{\mathrm{AB}}(\boldsymbol{k}) &= \begin{pmatrix} V/2 & 0 & 0 & f(\boldsymbol{k}) \\ 0 & V/2 & f^{*}(\boldsymbol{k}) & 0 \\ 0 & f(\boldsymbol{k}) & -V/2 & \gamma \\ f^{*}(\boldsymbol{k}) & 0 & \gamma & -V/2 \end{pmatrix}, \end{aligned} \tag{4}$$

where $f(\boldsymbol{k}) = -t_{||}(1 + \mathrm{e}^{\mathrm{i}\boldsymbol{k}\cdot\boldsymbol{a}_1} + \mathrm{e}^{\mathrm{i}\boldsymbol{k}\cdot\boldsymbol{a}_2})$ and $t_{||}$ describes the intralayer nearest neighbor hopping strength. Under the half filling constraint corresponding to one electron per lattice site, the chemical potential μ is zero. Since the unit cell of bilayer graphene includes four atoms, Green's function can be written as a 4×4 matrix. In the Matsubara formalism,[57] each element of the Green function matrix and its Fourier transformation are defined as

$$\begin{aligned} G_{\alpha\beta}(\boldsymbol{k},\tau) &= -\langle T_{\tau}(\alpha_{\boldsymbol{k}}(\tau)\beta^{\dagger}_{\boldsymbol{k}}(0))\rangle, \\ G_{\alpha\beta}(\boldsymbol{k},\mathrm{i}\omega_n) &= \int_0^{1/k_{\mathrm{B}}T} \mathrm{e}^{\mathrm{i}\omega_n\tau} G_{\alpha\beta}(\boldsymbol{k},\tau)\,\mathrm{d}\tau, \end{aligned} \tag{5}$$

where $\alpha_{\boldsymbol{k}}, \beta_{\boldsymbol{k}}$ refer to each fermionic annihilation operators $a_{1,\boldsymbol{k}}$, $b_{1,\boldsymbol{k}}$, $a_{2,\boldsymbol{k}}$, $b_{2,\boldsymbol{k}}$; τ is the imaginary time; $\omega_n = (2n+1)\pi k_{\mathrm{B}}T$ is the Fermionic Matsubara frequency;[57] T denotes the equilibrium temperature of the system; and k_{B} is the Boltzman constant. The Fourier transformation of the Green function matrix of the clean system ($\boldsymbol{G}^{(0)}$) can be readily obtained by the following equation:

$$\boldsymbol{G}^{(0)}_{\mathrm{AA(AB)}}(\boldsymbol{k},\mathrm{i}\omega_n) = \frac{1}{(\mathrm{i}\omega_n+\mu)\boldsymbol{1} - H^{\mathrm{T.B}}_{\mathrm{AA(AB)}}(\boldsymbol{k})}, \tag{6}$$

where $\boldsymbol{G}^{(0)}_{\mathrm{AA(AB)}}$ is the Green function of the clean system of AA (AB) stacked bilayer graphene. By substituting Eq. (4) into Eq. (6), the explicit form of the Green function matrix of the clean bilayer system is found for each stacking case. The explicit expression for each matrix element of the Green function is quite lengthy and not presented here. The electronic self-energy matrix of the disordered system in the presence of a finite but small density of impurity atoms, $n_i \ll 1$, can be obtained as[55]

$$\boldsymbol{\Sigma}(\mathrm{i}\omega_n) = \frac{n_{\mathrm{i}} v_{\mathrm{i}}}{1 - v_{\mathrm{i}}\overline{\boldsymbol{G}}_0(\mathrm{i}\omega_n)}, \tag{7}$$

where v_{i} denotes the electronic on-site energy, which shows the strength of the scattering potential. The local propagator of the clean system is given by

$$\overline{\boldsymbol{G}}_0(\mathrm{i}\omega_n) = \frac{1}{N}\sum_{\boldsymbol{k}} \boldsymbol{G}^{(0)}(\boldsymbol{k},\mathrm{i}\omega_n). \tag{8}$$

We replace the local bare Green function $\boldsymbol{G}_0(\mathrm{i}\omega_n)$ by the local full one ($\boldsymbol{G}(\mathrm{i}\omega_n)$) in Eq. (7), leading to the full self-consistent Born approximation. By neglecting the intersite correlations, the self-consistent problem requires the solution of the equation

$$\begin{aligned} \Sigma_{\alpha\alpha}(E) &= \frac{n_{\mathrm{i}} v_{\mathrm{i}}}{1 - v_{\mathrm{i}} G_{\alpha\alpha}(E)} \\ &= \frac{n_{\mathrm{i}} v_{\mathrm{i}}}{1 - v_{\mathrm{i}} G_{\alpha\alpha}(E + \mathrm{i}0^{+} - \Sigma(E))}, \end{aligned} \tag{9}$$

where $\alpha = A_1, B_1, A_2, B_2$. A simple analytical continuation as $\mathrm{i}\omega_n \longrightarrow E + \mathrm{i}0^{+}$ has been performed to obtain the retarded self-energy. The electronic self-energy should be found from a self-consistent solution of Eq. (9). The perturbative expansion for the Green function of both stacked disordered bilayer graphene is obtained via Dyson's equation[56]

$$\boldsymbol{G}(\boldsymbol{k},\mathrm{i}\omega_n) = \frac{1}{(\mathrm{i}\omega_n+\mu)\boldsymbol{1} - H^{\mathrm{T.B}}(\boldsymbol{k}) - \boldsymbol{\Sigma}(\mathrm{i}\omega_n)}, \tag{10}$$

where $H^{\mathrm{T.B}}$ refers to the model Hamiltonian in Eq. (4) for different stacking cases.

In the following, the expression for the electrical conductivity of bilayer graphene is presented using Green's function method.[56] The Kubo formula gives us the in-plane dynamical electrical conductivity (σ_{xx}) in terms of the correlation function between electrical currents[56]

$$\begin{aligned} &\Re\sigma_{xx}(\omega) \\ &= \lim_{\mathrm{i}\omega_n\to\omega+\mathrm{i}0^{+}} \Im\left(\int_0^{\beta} \mathrm{d}\tau \mathrm{e}^{\mathrm{i}\omega_n\tau}\langle T(J^{\mathrm{e}}_x(\tau)J^{\mathrm{e}}_x(0))\rangle\right), \end{aligned} \tag{11}$$

where J^{e}_x is the operator from of the electrical current, and $\omega_n = 2n\pi k_{\mathrm{B}}T$ is the bosonic Matsubara frequency. The electrical current operator has been derived based on the charge conservation equation. So current $\boldsymbol{J}^{\mathrm{e}}$ satisfies it as $\partial\rho/\partial t + \nabla\cdot\boldsymbol{J}^{\mathrm{e}} = 0$, where ρ is the density operator of electrons. Let us define the polarization operator $\boldsymbol{P}$ as[57]

$$\boldsymbol{P} = \sum_{l,m} \boldsymbol{R}^{\mathrm{c}}_m (a^{\dagger}_{l,m} a_{l,m} + b^{\dagger}_{l,m} b_{l,m}), \tag{12}$$

where $\boldsymbol{R}_m^{\rm c}$ denotes the position vector of the m-th unit cell in the honeycomb lattice, and $l = 1,2$ also denotes the layer in the lattice. The electrical current is readily obtained via $\boldsymbol{J}^{\rm e} = {\rm d}\boldsymbol{P}/{\rm d}t$. In terms of Fourier transformations of the creation and annihilation operators, the final expression for the electrical current operator for both types (AA and AB) along the x direction is given by

$$J_x^{\rm e} = {\rm i}t_{\parallel} \sum_{\boldsymbol{k},\boldsymbol{\delta}',l} \boldsymbol{i}\cdot\boldsymbol{\delta}'(a_{l,\boldsymbol{k}}^{\dagger} b_{l,\boldsymbol{k}}\, {\rm e}^{-{\rm i}\boldsymbol{k}\cdot\boldsymbol{\delta}'} + b_{l,\boldsymbol{k}}^{\dagger} a_{l,\boldsymbol{k}}\, {\rm e}^{-{\rm i}\boldsymbol{k}\cdot\boldsymbol{\delta}'}), \quad (13)$$

where $\boldsymbol{\delta}' = 0$, $\boldsymbol{a}_1$, $\boldsymbol{a}_2$ are the vectors connecting the nearest neighbor unit cells.

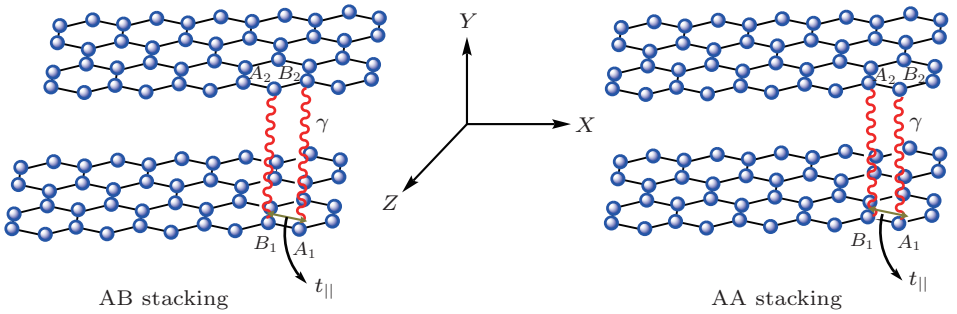


Fig. 1. (color online) The structure of bilayer. Both intra and inter layer hopping integrals are introduced in this figure.

After substituting Eq. (13) into Eq. (11), we can calculate the current–current correlation function within an approximation by implementing Wick's theorem. In order to calculate the correlation functions between the current operators, we apply the Lehman representation[58]

$$G_{\alpha\beta}(\boldsymbol{k}, {\rm i}\omega_n) = \int_{-\infty}^{\infty} \frac{{\rm d}E}{2\pi} \frac{\mathcal{A}_{\alpha\beta}(\boldsymbol{k},E)}{{\rm i}\omega_n - E}, \quad (14)$$

where $\mathcal{A}_{\alpha\beta}(\boldsymbol{k},E) = -2\Im G_{\alpha\beta}(\boldsymbol{k}, {\rm i}\omega_n \longrightarrow E + {\rm i}0^+)$ is the spectral function of the electronic system. Based on this representation, the Matsubara Green function can be related to the spectral function. Using Eq. (14) and performing Matsubara frequency summation, we obtain the final expression for the static electrical conductivity of AA stacking[59]

$$\begin{aligned}
\sigma_{\rm D.C.} &\equiv \Re\sigma_{xx}(\omega \longrightarrow 0) \\
&= \frac{3t_{\parallel}^2}{\pi} \int_{-\infty}^{+\infty} {\rm d}E \frac{{\rm d}(n_{\rm F}(E))}{{\rm d}E} \sum_{\boldsymbol{k}} \cos^2(k_y/2) \\
&\quad \times \Big[\cos(\sqrt{3}k_x) \Big(2\mathcal{A}_{B_1A_1}(\boldsymbol{k},E)\mathcal{A}_{B_1A_1}(\boldsymbol{k},E) \\
&\quad + 2\mathcal{A}_{A_1B_1}(\boldsymbol{k},E)\mathcal{A}_{A_1B_1}(\boldsymbol{k},E) \\
&\quad + \mathcal{A}_{B_1A_2}(\boldsymbol{k},E)\mathcal{A}_{B_2A_1}(\boldsymbol{k},E) \\
&\quad + \mathcal{A}_{B_2A_1}(\boldsymbol{k},E)\mathcal{A}_{B_1A_2}(\boldsymbol{k},E) \\
&\quad + \mathcal{A}_{A_1B_2}(\boldsymbol{k},E)\mathcal{A}_{A_2B_1}(\boldsymbol{k},E) \\
&\quad + \mathcal{A}_{A_2B_1}(\boldsymbol{k},E)\mathcal{A}_{A_1B_2}(\boldsymbol{k},E) \Big) \\
&\quad + 4\mathcal{A}_{A_1A_2}(\boldsymbol{k},E)\mathcal{A}_{A_1A_2}(\boldsymbol{k},E) \\
&\quad + \mathcal{A}_{A_1A_1}(\boldsymbol{k},E)\mathcal{A}_{A_2A_2}(\boldsymbol{k},E) \\
&\quad + \mathcal{A}_{B_2B_2}(\boldsymbol{k},E)\mathcal{A}_{B_1B_1}(\boldsymbol{k},E) \\
&\quad + \mathcal{A}_{B_1B_1}(\boldsymbol{k},E)\mathcal{A}_{B_2B_2}(\boldsymbol{k},E) \\
&\quad + \mathcal{A}_{B_1B_1}(\boldsymbol{k},E)\mathcal{A}_{A_1A_1}(\boldsymbol{k},E) \Big) \\
&\quad - 4\mathcal{A}_{A_1A_2}(\boldsymbol{k},E)\mathcal{A}_{A_1A_2}(\boldsymbol{k},E-\omega) \\
&\quad - \mathcal{A}_{A_1A_1}(\boldsymbol{k},E)\mathcal{A}_{A_2A_2}(\boldsymbol{k},E) \\
&\quad - \mathcal{A}_{B_2B_2}(\boldsymbol{k},E)\mathcal{A}_{B_1B_1}(\boldsymbol{k},E) \\
&\quad - \mathcal{A}_{B_1B_1}(\boldsymbol{k},E)\mathcal{A}_{B_2B_2}(\boldsymbol{k},E) \\
&\quad - \mathcal{A}_{B_1B_1}(\boldsymbol{k},E)\mathcal{A}_{A_1A_1}(\boldsymbol{k},E) \Big], \quad (15)
\end{aligned}$$

where $n_{\rm F}(x) = 1/({\rm e}^{x/k_{\rm B}T} + 1)$ is the Fermi–Dirac distribution function. The static electrical conductivity of the AB stacked bilayer graphene is obtained as

$$\begin{aligned}
\sigma_{\rm D.C.} &= t_{\parallel}^2 \int_{-\infty}^{+\infty} \frac{{\rm d}E}{2\pi} \frac{-{\rm d}n_{\rm F}(E)}{{\rm d}E} \\
&\quad \times \sum_k \delta_{1x}^2 \Big\{ \Big(2\cos(\sqrt{3}k_x)\cos(k_y) + \cos(\sqrt{3}k_x) \Big) \\
&\quad \times \Big(\mathcal{A}_{B_1A_1}^2(k,E) + \mathcal{A}_{A_1B_1}^2(k,E) \\
&\quad + \mathcal{A}_{B_2A_2}^2(k,E) + \mathcal{A}_{A_2B_2}^2(k,E) \\
&\quad + 2\mathcal{A}_{A_1B_2}(k,E)\mathcal{A}_{A_2B_1}(k,E) \\
&\quad + 2\mathcal{A}_{B_1A_2}(k,E)\mathcal{A}_{B_2A_1}(k,E) \Big) \\
&\quad - 4\Big(1 + \cos(k_y)\Big) \Big(\mathcal{A}_{A_1A_1}(k,E)\mathcal{A}_{B_1B_1}(k,E) \\
&\quad + \mathcal{A}_{A_1A_2}(k,E)\mathcal{A}_{B_2B_1}(k,E) \\
&\quad + \mathcal{A}_{A_2A_1}(k,E)\mathcal{A}_{B_1A_2}(k,E) \\
&\quad + \mathcal{A}_{A_1A_2}(k,E)\mathcal{A}_{B_2B_2}(k,E) \Big) \Big\}. \quad (16)
\end{aligned}$$

In the next section, the results of electrical conductivity for AA and AB stacked bilayer graphene are presented.

3. Results and discussion

We obtain the electrical conductivity of the impurity doped AA stacked bilayer graphene along the x direction, as shown in Fig. 2. Experimental studies of bilayer graphene have revealed exotic transport properties such as an anoma-

lous quantum Hall effect and finite temperature electrical conductivity at zero energy.[60–62] We implement a tight binding model Hamiltonian including a local energy term which describes the scattering of electrons from the impurity atoms. We obtain the electronic spectrum of the disordered tight binding model by the Green function approach, which gives the electrical conductivity by calculating the electrical current correlation function. The electronic self-energy of the disordered system is calculated within a self-consistent solution of Eq. (9). The process is started with an initial guess for $\Sigma_{\alpha\alpha}(E)$ and is repeated until the convergence is reached. The final results for the self-energy matrix elements are employed to obtain the electronic Green function of the disordered bilayer graphene. Afterwards, the static electrical conductivity is calculated using Eqs. (15) and (16). For obtaining the numerical results of conductivity, the intralayer nearest neighbor hopping parameter ($t_{\|}$) is set to 1. Therefore, the other parameters in the model Hamiltonian are expressed as $\gamma/t_{\|}$, $V/t_{\|}$, $v_{\rm i}/t_{\|}$, $\mu/t_{\|}$. Moreover, in our calculations, σ_0 is the minimal conductivity of graphene.

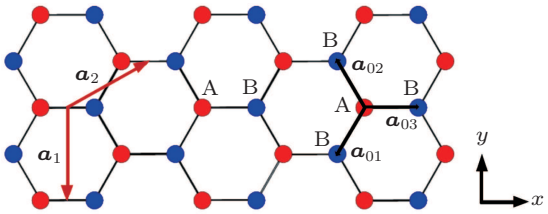


Fig. 2. (color online) The honeycomb structure. The light dashed lines denote the Bravais lattice unit cell. Each cell includes two nonequivalent sites, which are indicated by A and B. $\boldsymbol{a}_1$ and $\boldsymbol{a}_2$ are the primitive vectors of the unit cell. $\boldsymbol{a}_{01}$, $\boldsymbol{a}_{02}$, and $\boldsymbol{a}_{03}$ are three vectors that connect the nearest neighbor sites.

In Fig. 3, we present the in-plane electrical conductivity of the biased AA stacked bilayer graphene versus impurity concentration $n_{\rm i}$ for different bias voltages, namely, $V/t_{\|} = 0.0, 0.5, 1.0, 2.0, 3.0$ for fixed electron-impurity scattering amplitude $v_{\rm i}/t = 0.3$. The increase of the impurity concentration reduces electrical conductivity $\sigma_{xx-{\rm AA}}$ at a given bias voltage $V/t_{\|}$. This behavior can be understood from the fact that the increase of impurity concentration $n_{\rm i}$ leads to the increase of the scattering rate of electrons from the impurity atoms, which decreases the electrical conductivity. In addition, at a fixed impurity concentration $n_{\rm i}$, the electrical conductivity of the AA stacked bilayer graphene is the same for $V/t_{\|} = 0, 0.5, 1.0$. In other words, the plots for bias voltages $V/t_{\|} = 0, 0.5, 1.0$ fall on each other on the whole range of impurity concentrations. In Fig. 3, it is clearly observed that the electrical conductivity reduces with increasing bias voltage for $V/t_{\|} > 1.0$. A drastic reduction takes place at $V/t_{\|} = 3.0$.

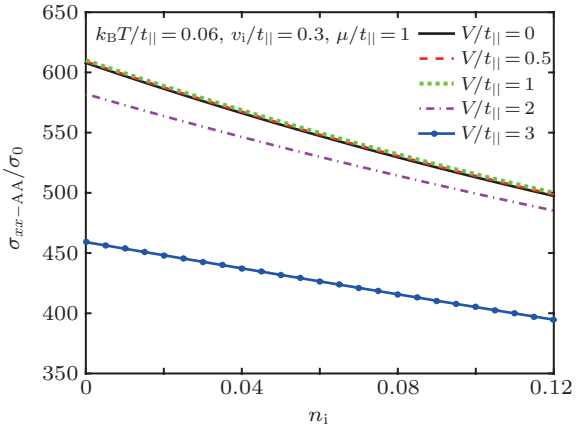


Fig. 3. (color online) Normalized electrical conductivity σ_{xx}/σ_0 of biased doped AA stacked bilayer graphene as a function of impurity concentration $n_{\rm i}$ for different bias voltages $V/t_{\|}$ for $v_{\rm i}/t_{\|} = 0.3$. The normalized temperature is assumed to be $k_{\rm B}T/t_{\|} = 0.06$.

The effect of the impurity concentration on the temperature behavior of the electrical conductivity of the AA stacked bilayer graphene in the presence of bias voltage $V/t = 0.6$ for $v_{\rm i}/t_{\|} = 0.3$ is shown in Fig. 4. This figure shows a uniform behavior of the temperature dependence of the electrical conductivity. However, at a fixed temperature, lower impurity concentration $n_{\rm i}$ causes less scattering of electrons from the impurity atoms, which leads to a higher electrical conductivity.

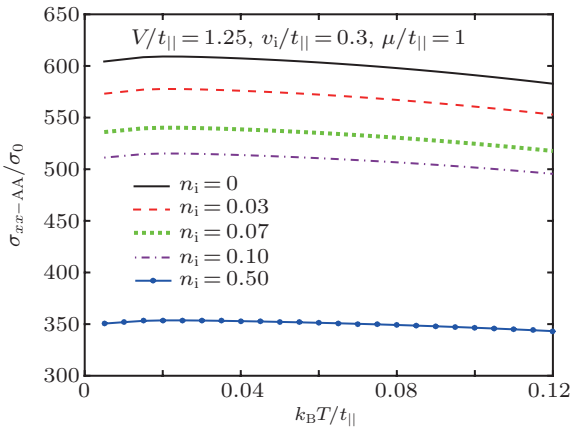


Fig. 4. (color online) Normalized electrical conductivity σ_{xx}/σ_0 of biased doped AA stacked bilayer graphene as a function of temperature $k_{\rm B}T/t_{\|}$ for different impurity concentrations $n_{\rm i}$ for $v_{\rm i}/t_{\|} = 0.3$. The normalized chemical potential is assumed to be $\mu/t_{\|} = 1.0$.

In Fig. 5, we plot the static electrical conductivity $\sigma_{\rm AA-stacked}/\sigma_0$ of the biased AA stacked bilayer graphene versus normalized temperature $k_{\rm B}T/t_{\|}$ for different impurity potential strengths, namely, $v_{\rm i}/t_{\|} = 0, 0.2, 0.4, 0.6$ with $V/t_{\|} = 1.25$. This plot indicates that the electrical conductivity is nonzero at zero temperature for every $v_{\rm i}/t_{\|}$. There is also a peak in the electrical conductivity which locates at $k_{\rm B}T/t_{\|} = 0.02$ for all values of $v_{\rm i}/t_{\|}$. Figure 5 shows that upon increase of the temperature, $\sigma_{\rm AA-stacked}/\sigma_0$ increases until it reaches a maximum and then decreases. The increasing behavior of the electrical conductivity comes from the fact that

the temperature causes more electronic transitions. For temperatures above the peak position, we observe a decreasing behavior of the electrical conductivity, which is related to the increase of the scattering rate of electrons. Moreover, at a fixed temperature, the increase of the potential scattering leads to more scattering between electrons and the impurity atoms and the conductivity reduces. The novel feature in Fig. 5 is that the electrical conductivity curves of the AA stacked bilayer graphene for two potential strengths $v_i/t_{\|} = 0.4, 0.6$ fall on each other in the temperature range $k_B T/t_{\|} < 0.08$. For the normalized temperature above 0.08, the electrical conductivity for $v_i/t_{\|} = 0.4$ is higher compared to that for $v_i/t_{\|} = 0.6$.

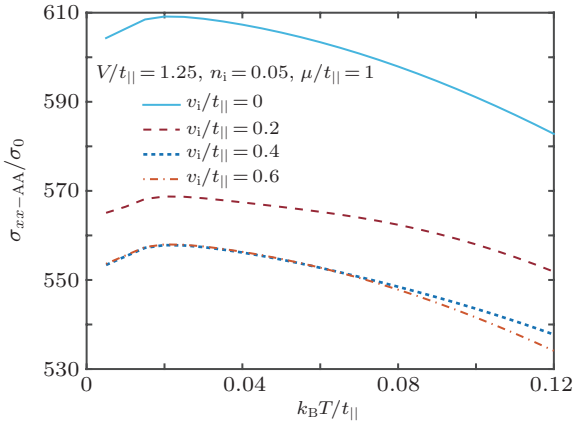


Fig. 5. (color online) Normalized electrical conductivity σ_{xx}/σ_0 of biased doped AA stacked bilayer graphene as a function of temperature $k_B T/t_{\|}$ for different scattering strengths $v_i/t_{\|}$ for $n_i = 0.05$. The normalized bias voltage is assumed to be $V/t_{\|} = 1.25$.

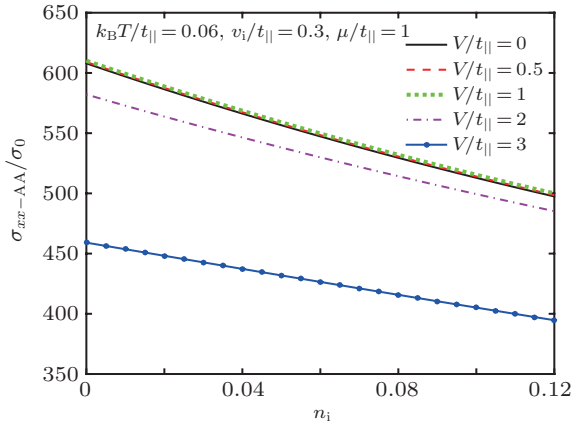


Fig. 6. (color online) Normalized electrical conductivity σ_{xx}/σ_0 of biased doped AB stacked bilayer graphene as a function of impurity concentration n_i for different bias voltages $V/t_{\|}$ for $v_i/t_{\|} = 0.3$. The normalized temperature is assumed to be $k_B T/t_{\|} = 0.06$.

The electrical conductivity of the AB stacked bilayer graphene ($\sigma_{\mathrm{AB-stacked}}/\sigma_0$) versus the impurity concentration for different bias voltages at $k_B T/t_{\|} = 0.06$ is shown in Fig. 6. This figure implies that impurity concentration n_i has no remarkable effect on the electrical conductivity for $V/t_{\|} > 1.5$. In other words, the electrical conductivity presents a uniform behavior in terms of n_i for $V/t_{\|} > 1.5$. However, this is not the case for $V/t_{\|} < 1.5$, where $\sigma_{\mathrm{AA-stacked}}/\sigma_0$ decreases with n_i at a fixed temperature.

We have also studied the effect of impurity concentration n_i on the temperature behavior of $\sigma_{\mathrm{AB-stacked}}/\sigma_0$. In Fig. 7, we plot the electrical conductivity of the AB stacked bilayer graphene versus the temperature for different impurity concentrations, namely, $n_i = 0, 0.03, 0.07, 0.1, 0.2, 0.5$ with $V/t_{\|} = 1.25$ and $v_i/t_{\|} = 0.3$. Uniform behavior in the temperature dependence of electrical conductivity $\sigma_{\mathrm{AB-stacked}}/\sigma_0$ is clearly observed for all impurity concentrations. In addition, at a fixed temperature, lower impurity concentration causes less scattering of electrons from the impurities, which leads to a higher electrical conductivity.

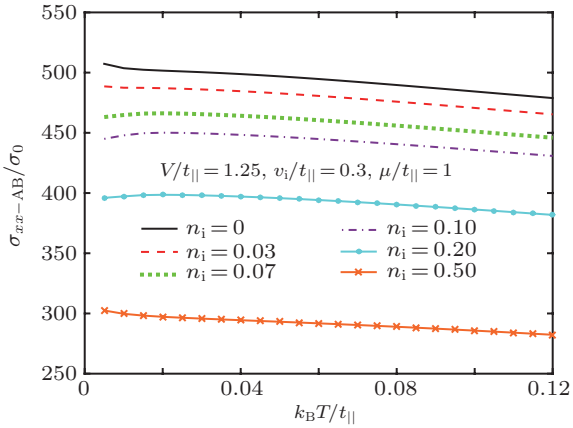


Fig. 7. (color online) Normalized electrical conductivity σ_{xx}/σ_0 of biased doped AB stacked bilayer graphene as a function of temperature $k_B T/t_{\|}$ for different impurity concentrations n_i for $v_i/t_{\|} = 0.3$. The normalized chemical potential is assumed to be $\mu/t_{\|} = 1.0$.

In Fig. 8, we present the electrical conductivity of the AB stacked bilayer graphene versus normalized temperature $k_B T/t_{\|}$ for different scattering potential strengths with $n_i = 0.05$ at $V/t_{\|} = 1.25$. The increases of temperature increases the scattering between electrons and the impurity atoms, which consequently reduces the electrical conductivity, as shown in Fig. 8. Moreover, the electrical conductivity decreases with the scattering potential strength $v_i/t_{\|}$.

Finally, we study the effect of the chemical potential on the impurity potential strength dependence of the electrical conductivity of the AB stacked bilayer graphene, and the main results are presented in Fig. 9. In this figure, we plot the electrical conductivity of the AB stacked bilayer graphene ($\sigma_{\mathrm{AB-stacked}}/\sigma_0$) versus impurity potential strength $v_i/t_{\|}$ for different chemical potentials, namely, $\mu/t_{\|} = 0, 0.3, 0.8, 1.5, 2.5, 4$ with $V/t_{\|} = 1.25$ at fixed temperature $k_B T/t_{\|} = 0.06$. Figure 9 indicates that the scattering strength has no remarkable effect on the electrical conductivity for each chemical potential. Therefore, we observe a uniform behavior for all curves in Fig. 9. On the other hand, at fixed $v_i/t_{\|}$, the electrical conductivity increases with chemical potential in the region $\mu/t_{\|} < 0.8$. It can be understood from the fact

that the increase of the chemical potential raises the electronic transitions from the ground state to the excited states, which causes the increase of $\sigma_{\mathrm{AB-stacked}}/\sigma_0$. Thus, we can expect that the electrical conductivity decreases with $\mu/t_{\|}$. Upon further increase of the chemical potential above 0.8, the rate of scattering between electrons enhances and consequently the electrical conductivity reduces. Based on Fig. 9, we find that $\sigma_{\mathrm{AB-stacked}}/\sigma_0$ vanishes for $\mu/t_{\|} = 0, 2.5, 4.0$.

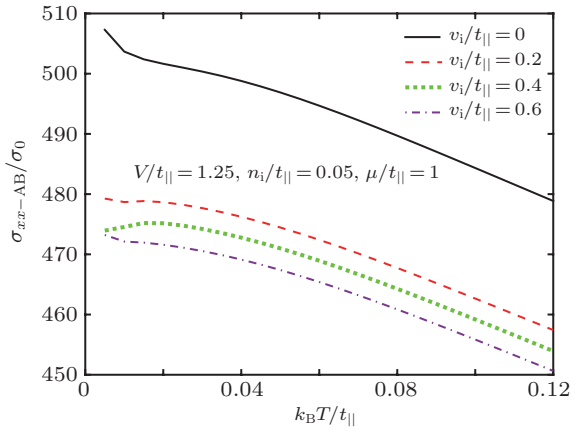


Fig. 8. (color online) Normalized electrical conductivity σ_{xx}/σ_0 of biased doped AB stacked bilayer graphene as a function of temperature $k_{\mathrm{B}}T/t_{\|}$ for different scattering strengths $v_{\mathrm{i}}/t_{\|}$ for $n_{\mathrm{i}} = 0.05$. The normalized bias voltage is assumed to be $V/t_{\|} = 1.25$.

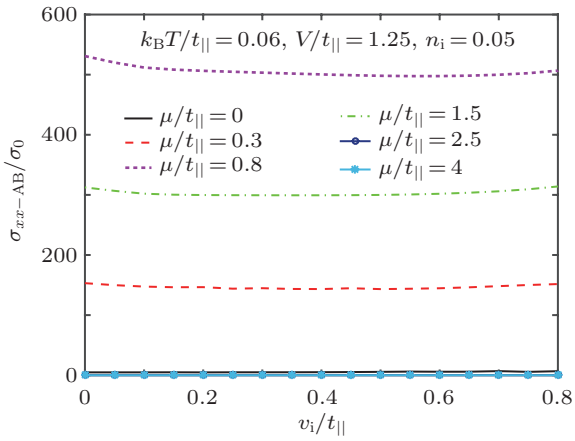


Fig. 9. (color online) Normalized electrical conductivity σ_{xx}/σ_0 of biased doped AB stacked bilayer graphene as a function of normalized scattering strength $v_{\mathrm{i}}/t_{\|}$ for different chemical potentials $\mu/t_{\|}$ for $n_{\mathrm{i}} = 0.05$. The normalized temperature is assumed to be $k_{\mathrm{B}}T/t_{\|} = 0.06$.

4. Summary

We have presented the electrical conductivity of both simple and bernal stacked biased bilayer graphene in the presence of impurity atoms. With the tight binding model Hamiltonian including a local energy term, the electronic excitation spectrum has been studied. Using the self-consistent Born approximation and the linear response theory, the electrical conductivity of disordered bilayer graphene has been obtained. Specially, the effects of the impurity concentration and the scattering strength on the temperature dependence of conductivity have been investigated. We find that the electrical conductivity decreases with increasing impurity concentration for all values of scattering potential strength. The results also show that there is a peak in the electrical conductivity in terms of temperature for all scattering strengths.

References

[1] McCann E and Fal'ko V I 2006 *Phys. Rev. Lett.* **96** 086805
[2] Novoselov K S 2006 *Nat. Phys.* **2** 177
[3] Novoselov K S 2005 *Nature* **438** 197
[4] Zhang Y, Tan Y W, Stormer H L and Kim P 2005 *Nature* **438** 201
[5] Koshino M and Ando T 2006 *Phys. Rev. B* **73** 245403
[6] Nilsson J, Castro Neto A H, Guinea F and Peres N M R 2008 *Phys. Rev. B* **78** 045405
[7] Cserti J, Csord'as A and D'avid G 2007 *Phys. Rev. Lett.* **99** 66802
[8] Min H, Sahu B, Banerjee S K and MacDonald A H 2007 *Phys. Rev. B* **75** 155115
[9] Castro Neto A H, Guinea F, Peres N M R, Novoselov K S and Geim A K 2009 *Rev. Mod. Phys.* **81** 109
[10] Weitz R T, Allen M T, Feldman B E, Martin J and Yacoby A 2010 *Science* **330** 812
[11] Lemonik Y, Aleiner I L, Toke C and Fal'ko V I 2010 *Phys. Rev. B* **82** 201408
[12] Castro E V, Peres N M R, Stauber T and Silva N A P 2008 *Phys. Rev. Lett.* **100** 186803
[13] Nandkishore R and Levitov L 2010 *Phys. Rev. Lett.* **104** 156803
[14] Zhang F, Min H, Polini M and MacDonald A H 2010 *Phys. Rev. B* **81** 041402
[15] Vafek O and Yang K 2010 *Phys. Rev. B* **81** 041401
[16] Guinea F, Castro Neto A H and Peres N M R 2006 *Phys. Rev. B* **73** 245426
[17] Ohta T, Bostwick A, Seyller T, Horn K and Rotenberg E 2006 *Science* **313** 951
[18] McCann E 2006 *Phys. Rev. B* **74** 161403(R)
[19] Oostinga J B, Heersche H B, Liu X, Morpurgo A F and Vandersypen L M K 2007 *Nat. Mater.* **7** 151
[20] Castro E V 2007 *Phys. Rev. Lett.* **99** 216802
[21] Novoselov K S, Fal'ko V I, Colombo L, Gellert P R, Schwab M G and Kim K 2012 *Nature* **490** 192
[22] Dean C R, Young A F, Meric I, Lee C, Wang L, Sorgenfrei S, Watanabe K, Taniguchi T, Kim P, Shepard K L and Hone J 2010 *Nat. Nanotech.* **5** 722
[23] Novoselov K S, Geim A K, Morozov S V, Jiang D, Zhang Y, Dubonos S V, Grigorieva I V and Firsov A A 2004 *Science* **306** 666
[24] Novoselov K S, McCann E, Morozov S V, Fal'ko V I, Katsnelson M I, Zeitler U, Jiang D, Schedin F and Geim A K 2006 *Nat. Phys.* **2** 177
[25] Ghosh S, Bao W, Nika D L, Subrina S, Pokatilov E P, Lau C N and Balandin A A 2010 *Nat. Mater.* **9** 555
[26] Balandin A A 2011 *Nat. Mater.* **10** 569
[27] Neek-Amal M and Peeters F M 2010 *Phys. Rev. B* **81** 235421
[28] Zhang Y Y, Wang C M, Cheng Y and Xiang Y 2011 *Carbon* **49** 4511
[29] Nair R R, Blake P, Grigorenko A N, Novoselov K S, Booth T J, Stauber T, Peres N M R and Geim A K 2008 *Science* **320** 1308
[30] Bunch J S, Verbridge S S, Alden J S, an der Zande A M, Parpia J M, Craighead H G and McEuen P L 2008 *Nano Lett.* **8** 2458
[31] Elias D C, Nair R R, Mohiuddin T M G, Morozov S V, Blake P, Halsall M P, Ferrari A C, Boukhvalov D W, Katsnelson M I, Geim A K and Novoselov K S 2009 *Science* **323** 610
[32] Bae S, Kim H, Lee Y, Xu X, Park J S, Zheng Y, Balakrishnan J, Lei T, Kim H R, Song Y I, Kim Y J, Kim K S, Ozyilmaz B, Ahn J H, Hong B H and Iijima S 2010 *Nat. Nanotech.* **5** 574
[33] Xia F, Farmer D B, Lin Y M and Avouris P 2010 *Nano Lett.* **10** 715
[34] Wang C R, Lu W S, Hao L, Lee W L, Lee T K, Lin F, Cheng I C and Chen J Z 2011 *Phys. Rev. Lett.* **107** 186602
[35] Yan H, Li X, Chandra B, Tulevski G, Wu Y, Freitag M, Zhu W, Avouris P and Xia F 2012 *Nat. Nanotech.* **7** 330
[36] Yan J, Kim M H, Elle J A, Sushkov A B, Jenkins G S, Milchberg H M, Fuhrer M S and Drew H D 2012 *Nat. Nanotech.* **7** 472

[37] Sugawara K, Kanetani K, Sato T and Takahashi T 2011 *AIP Adv.* **1** 022103
[38] Kanetani K, Sugawara K, Sato T, Shimizu R, Iwaya K, Hitosugi T and Takahashia T 2012 *Proc. Natl. Acad. Sci. USA* **109** 19610
[39] Gong L, Young R J, Kinloch I A, Riaz I, Jalil R and Novoselov K S 2012 *ACS Nano* **6** 2086
[40] Young R J, Kinloch I A, Gong L and Novoselov K S 2012 *Compos. Sci. Technol.* **72** 1459
[41] Geim A K and Novoselov K S 2007 *Nat. Mater.* **6** 183
[42] Oostinga J B, Heersche H B, Liu X, Morpurgo A F and Vandersypen L M K 2007 *Nat.* Mat.
[43] Milton Pereira J J, Vasilopoulos P and Peeters F M 2007 *Nano Lett.* **7** 946
[44] Nilsson J, Castro Neto A H, Guinea F, and Peres N M R 2007 *Phys. Rev. B* **76** 165416
[45] Katsnelson M I 2007 *Phys. Rev. B* **76** 073411
[46] Kechedzhi K, Falko V I, McCann E and Altshuler B L 2007 *Phys. Rev. Lett.* **98** 176806
[47] Gorbachev R V, Tikhonekov F V, Mayorov A S, Horsell D W and Savchenko A K 2007 *Phys. Rev. Lett.* **98** 176805
[48] Hao L and Lee T K 2010 *Phys. Rev. B* **81** 165445
[49] Rezania H and Yarmohammadi M 2016 *Superlattices and Microstructures* **89** 15
[50] Rezania H and Yarmohammadi M 2016 *Physica E* **75** 125
[51] Zhou S Y, Gweon G H and Lanzara A 2006 *Annals of Physics* **321** 1730
[52] Ohta T, Bostwick A, Seyller T, Horn K and Rotenberg E 2006 *Science* **313** 951
[53] Mallet P, Varchon F, Naud C, Magaud L, Berger C and Veuillen J Y 2007 *Phys. Rev. B* **76** 041403
[54] Li G and Andrei E V 2007 *Nat. Phys.* **3** 623
[55] Doniach S and Sondheimer E H 1988 Green's Function for Solid State Physicists (Singapour: World Scientific) p. 125
[56] Mahan G D 1993 *Many Particle Physics* (New York: Plenumn Press) p. 123
[57] Nilsson J, Castro A H, Guinea F and Peres N M 2006 *Phys. Rev. Lett.* **97** 266801
[58] Fetter A L and Walecka J D 1971 *Quantum Theory of Many Particle Systems* (New York: MacGraw-Hill) p. 130
[59] Rezania H and Abdi A 2015 *Euro. Phys. J. B* **88** 173
[60] Cserti J 2007 *Phys. Rev. B* **75** 033405
[61] Cserti J, Csordas A and David G 2007 *Phys. Rev. Lett.* **99** 066802
[62] Ohta T, Bostwick A, McChesney J L, Seyller T, Horn K and Rotenberg E 2007 *Phys. Rev. Lett.* **98** 206802